

Dynamic Spin Correlation Function of the Alternating Spin-1/2 Antiferromagnetic Chain with Competing Interactions

Shigeyoshi MORI, Isao HARADA¹ * and Takashi TONEGAWA²

Department of Physics, Fukuyama University, Fukuyama 729-02,

¹*Department of Physics, Faculty of Science, Okayama University, Okayama 700*

²*Department of Physics, Faculty of Science, Kobe University, Rokkodai, Kobe 657*

(Received

)

Dynamic spin correlation function of the $S = 1/2$ antiferromagnetic spin chain with alternating nearest neighbor and competing next nearest neighbor interactions is studied using the numerical diagonalization method. We find characteristics of the correlation function, which are the consequence of the dimer order in the ground state: (1) A typical singlet-triplet gap is observed and such a lowest-energy triplet state is found to form a bound state, showing strong peaks below a continuum band with weak but distinct upper and lower boundaries. (2) The intensity of the bound state shows a quite different wavevector-dependence from that of the corresponding intensity at the lower boundary in the usual antiferromagnet. These features are examined by the variational calculation and are favorably discussed in connection with recent experimental results of neutron inelastic scattering in the inorganic spin-Peierls system, CuGeO₃.

KEYWORDS: dynamic spin correlation function, dimer order, singlet-triplet energy gap, spin-Peierls system, CuGeO₃

§1. Introduction

It is realized recently that a spin gap due to the singlet spin dimer is rather common features in low dimensional quantum spin systems and plays important roles in the mechanism of the oxide superconductor. The spin-Peierls order, which is a consequence of the combined effects of the lattice distortion and the singlet dimer, is one of the highlights in this field and has attracted a renewed interest since the discovery of the inorganic Cu compound, CuGeO₃.¹⁾

Because of large and high-quality samples, it becomes able to perform neutron inelastic scattering (NIS) for CuGeO₃,^{2,3)} which yields invaluable information on the dynamic properties of the spin-Peierls system. We believe that this is the most important progress in experiments comparing with the situation in organic materials about 15 years ago.⁴⁾ According to the experimental results, the dynamic spin correlation function seems to be, at least at a first glance, very similar to that of the typical one-dimensional antiferromagnet. It is, however, realized several important differences: (1) At the wavevectors $Q = 0$ and π in units of $1/a$ where a is the lattice constant in the uniform phase, it exhibits a typical gap. (2) In the whole wavevector space, bound state peaks seem to exist below the continuum band which has a rather distinct lower boundary.³⁾ (3) The intensity of the bound state decreases with decreasing Q from π but the decreasing rate is much slower than that in the typical one-dimensional antiferromagnet.²⁾

It is the purpose of this paper to reveal characteristics of the dynamic spin correlation function of the one-

dimensional quantum spin chain which has the dimer order in the ground state.⁵⁾ We do not aim, at present, at making a quantitative comparison with the experimental results but want to clarify the characteristic features of the correlation function of the system described by the following Hamiltonian:

$$\mathcal{H} = \sum_n [(1 + (-1)^n \delta) \mathbf{S}_n \cdot \mathbf{S}_{n+1} + j \mathbf{S}_n \cdot \mathbf{S}_{n+2}], \quad (1.1)$$

where \mathbf{S}_n represents the spin-1/2 operator at the n th site. $\delta (1 \geq \delta \geq 0)$ is the parameter describing the bond-alternation and $j (> 0)$ is the strength of the next nearest neighbor (nnn) interaction divided by that of the nearest neighbor (nn) interaction which is set to be unity. This Hamiltonian is believed to be appropriate for CuGeO₃,^{6,7)} although the parameter values for it are still controversial.

The ground-state phase diagram of the system described by the Hamiltonian (1.1) is shown in Fig. 1,^{8,9)} where the space is spanned by the two parameters, δ and j , both of which lead cooperatively to the dimer ground state with an excitation gap. As is seen in Fig. 1, the dimer order (D) takes place everywhere except for the $\delta = 0$ and $j < j_c (\simeq 0.24)$ ^{10,11)} line, where the ground state is the usual gapless spin fluid (SF) state as in the case of $\delta = 0$ and $j = 0$. On the disorder line, $\delta = -2j + 1$, which is shown by the dashed line in Fig. 1, the ground state is the direct product of the singlet dimers of nn spins so that a spin correlates only with the other spin in the dimer. As the ground state on this disorder line is a prototype of the dimer order, we focus our attention in this paper mainly on the dynamic spin correlation function in the case of the dimer ground state on this disorder line, which starts from the

* E-mail: harada@cc.okayama-u.ac.jp

independent dimer point, $(\delta = 1, j = 0)$, and ends at the point, $(\delta = 0, j = 0.5)$, called the Majumdar-Ghosh (MG) point. It is worth noticing that the dimer ground states are doubly degenerate¹²⁾ on the line, $\delta = 0$ and $j > j_c$, due to the translational symmetry of the Hamiltonian while a finite value of δ lifts the degeneracy. This observation leads us to the fact that there is a domain wall excitation in the former case but not in the latter case, as will be discussed in the following sections.

In the next section, we describe our numerical method to reproduce the dynamic spin correlation function and present the result with some discussions. The variational calculation is introduced in §3 to extract a physical picture from the numerical result. The last section is devoted to our conclusion.

§2. Numerical Calculation

In this section, we first summarize briefly the numerical method developed by Gagliano and Balseiro,¹³⁾ which enables us to calculate the dynamic spin correlation function $\mathcal{S}^{zz}(Q, \omega)$, making this paper self-contained. Then, the result of $\mathcal{S}^{zz}(Q, \omega)$ will be presented in a graphical form and its characteristics will be discussed.

We define $\mathcal{S}^{zz}(Q, \omega)$ by

$$\begin{aligned} \mathcal{S}^{zz}(Q, \omega) &= \frac{1}{2\pi} \int_{-\infty}^{\infty} dt e^{-i\omega t} \langle 0 | S_{-Q}^z S_Q^z(t) | 0 \rangle \quad (2.1) \\ &= \frac{1}{\pi} \lim_{\epsilon \rightarrow +0} \\ &\quad \times \text{Im}[\langle 0 | S_{-Q}^z(\omega - i\epsilon + E_0 - \mathcal{H})^{-1} S_Q^z | 0 \rangle], \quad (2.2) \end{aligned}$$

where

$$S_Q^z = N^{-1/2} \sum_n \exp(iQn) S_n^z, \quad (2.3)$$

$$S_Q^z(t) = \exp(i\mathcal{H}t) S_Q^z \exp(-i\mathcal{H}t), \quad (2.4)$$

$\text{Im}[\dots]$ means the imaginary part and $|0\rangle$ denotes the ground state, which is obtained using the numerical diagonalization method with the standard Lanczos algorithm. Once the ground state of a finite system is obtained, then $\mathcal{S}^{zz}(Q, \omega)$ can be calculated using the continued fraction expansion (CFE) for the resolvent in the tridiagonal basis of the Hamiltonian with the initial vector $S_Q^z |0\rangle$. The tridiagonal expansion of the Hamiltonian can be carried out numerically again with the Lanczos algorithm. Then, we obtain spectral weights and poles of the $\mathcal{S}^{zz}(Q, \omega)$ with the CFE representation up to the order of 70. The convergence of the spectral weights and the pole positions are rather rapid in the low energy excitations, while it is worse in high energy excitations although they have only weak spectral weights.

In Fig. 2, we present our numerical results of the dynamic correlation function $\mathcal{S}^{zz}(Q, \omega)$ for $N = 24$ for several parameter values on the disorder line together with the result of an exceptional case, the antiferromagnetic chain ($j = 0$ and $\delta = 0$), for comparison.

In Fig. 2 (a), we show a typical $\mathcal{S}^{zz}(Q, \omega)$ for the nn Heisenberg antiferromagnet. The spectrum consists of the continuum band with the lower and the upper boundaries, which coincide with the known curves, $\omega_L =$

$(\pi/2)\sin(Q)$ and $\omega_U = \pi\sin(Q/2)$, respectively. We note that the intensity is distributed within the band although the intensity at the lower boundary is high and seems to diverge especially at $Q = \pi$. The result agrees with the one known for this system, showing the validity of our numerical calculation, although our spectra consist of the discrete poles due to the finiteness of the system size.

Now we proceed in cases where the ground state has the dimer order. We especially focus our attention on the perfect dimer cases, which occur on the disorder line as was mentioned in §1. The first example is the independent dimer point at which $\mathcal{S}^{zz}(Q, \omega)$ shows the delta function shape at $\omega = 2$ without dispersion. It is easy to understand this since each isolated dimer has the singlet-triplet gap of 2 in our units. A bulk triplet state is obviously the state where one of $N/2$ nn singlet dimers in the ground state is excited to the triplet state. As δ decreases and j increases, the degeneracy of these states is lifted and these states result in forming the triplet band, since the dimer propagates and spreads out due to the weak nn and nnn interactions. We show in Fig. 2 (b) an example of $\mathcal{S}^{zz}(Q, \omega)$ for this category, where the excited triplet states have a little dispersion. It is interesting to note that the state which consists of a linear combination of such states with the wavevector $\pi/2$ is the exact eigenstate of the Hamiltonian as far as the parameters are on the disorder line.¹⁴⁾

At another end of the disorder line, the MG point, it is known that the triplet states form a band whose elementary excitation is a domain wall connecting two degenerate ground states.¹²⁾ We note that the situation occurs only if $\delta = 0$. In Fig. 2 (d) the bound state predicted can be seen in the vicinity of $Q = \pi/2$ and seems to merge into the lower boundary of the continuum band at a certain wavevector. This observation is again consistent with the known result.¹²⁾

The most typical spectrum of the dynamical correlation function on the disorder line can be seen in Fig. 2 (c) and it also seems to be appropriate for the discussion of NIS in CuGeO₃. First of all, we want to note that the lowest pole for each wavevector is isolated from others. Although the situation is smeared by the finite-size effect, we confirm this statement by the analysis of the size dependence of the positions and the spectral weights of such poles. This suggests that the lowest poles form the bound state splitting off from the triplet continuum band, which has rather distinct lower and upper boundaries.

Last point we would like to mention in this section is the wavevector dependence of the intensities at the lowest energy poles ω_B , which is shown in Fig. 3. In this figure $\mathcal{S}^{zz}(Q, \omega_B)/\mathcal{S}^{zz}(\pi, \omega_B)$ for $j = 0.3$ is plotted as a function of Q . We note that the denominator $\mathcal{S}^{zz}(\pi, \omega_B)$ itself decreases rather rapidly when δ is introduced and the intensity is distributed to other wavevector modes. In addition, the higher energy tail shrinks as δ increases so that the intensity at the lowest energy mode seems to have a relatively high intensity. Especially, at $Q = \pi/2$ the width becomes zero, so that the intensity can be comparable with that at $Q = \pi$. This behavior of the intensities at the lowest energy poles is consistent with

the experimental observation.

In the next section, we develop the variational calculation, emphasizing an important role of the local triplet dimer in the singlet dimer background, to make clear the nature of the triplet excitations studied in this section.

§3. Variational Calculation

In this section, we pursue a variational calculation for the excited triplet states, assuming the complete dimer singlet ground state, in order to gain insights into the nature of the triplet bound state as well as of the triplet continuum band, which have been shown in the previous section.

Before going into the detailed calculation, we consider how to construct appropriate variational states. The most plausible explanation for the low energy excited states in the system seems to be the one based on the domain wall scenario like in the case of the MG point.¹²⁾ However, we note, when we introduce the alternation, the domain wall is no longer an elementary excitation of the system since the ground-state degeneracy is lifted by the alternation. We suppose the following two types of the states as our variational states: (1) For the triplet bound state, we adopt the state in which one of $N/2$ singlet dimers in the dimer ground state is excited to the triplet dimer. (2) For the triplet band states, we consider the states in which two triplet dimers among $N/2 - 2$ singlet dimers couple into triplet. Note that the former state is nothing but an extreme state of the two domain wall states, where two domain walls are located on nn sites. It is clear that these states are the low-lying eigenstates in the independent dimer limit ($\delta = 1, j = 0$).

Based on the observation above, we build up the variational states. For convenience, we employ the two-spin states on a stronger bond of a nn pair as local bases of the Hamiltonian. Then, the following symbols are introduced for the singlet state and the three components of the triplet state:

$$\begin{aligned} |\bullet_n\rangle &\equiv 2^{-1/2} |\uparrow_n \downarrow_{n+1} - \downarrow_n \uparrow_{n+1}\rangle, \\ |\downarrow_n\rangle &\equiv |\uparrow_n \uparrow_{n+1}\rangle, \\ |\circ_n\rangle &\equiv 2^{-1/2} |\uparrow_n \downarrow_{n+1} + \downarrow_n \uparrow_{n+1}\rangle, \\ | -1_n\rangle &\equiv |\downarrow_n \downarrow_{n+1}\rangle, \end{aligned}$$

where n denotes the site and is assumed to be the even number. For example, the dimer ground state is expressed by $|D\rangle = |\cdots \bullet \bullet \bullet \cdots\rangle$. We choose the following orthonormal states as the variational bases for the low energy triplet states with the wavevector Q :

$$|a_Q\rangle \equiv (2/N)^{1/2} \sum_n e^{iQm} |a_m\rangle, \quad (3.1)$$

$$|b_{q_1, q_2}\rangle \equiv C(q_1, q_2) \sum_{m,n} [e^{i(q_1 m + q_2 n)} - e^{i(q_1 n + q_2 m)}] |b_{m,n}\rangle, \quad (3.2)$$

where $Q = q_1 + q_2$, and $C(q_1, q_2)$ denotes the normalization constant, and

$$|a_m\rangle = |\cdots \bullet \bullet 1_m \bullet \bullet \cdots\rangle, \quad (3.3)$$

$$|b_{m,n}\rangle = |\cdots \bullet \bullet 1_m \bullet \bullet \cdots \circ_n \bullet \bullet \cdots\rangle. \quad (3.4)$$

These $|a_m\rangle$ and $|b_{m,n}\rangle$ are depicted in Fig. 4. It is notable that two triplet states, $|b_{m,n}\rangle$ and $|b_{n,m}\rangle$, are superimposed antisymmetrically so as to produce the $S = 1$ continuum states. In addition, we deal only with the triplet states with $S_t^z \equiv \sum_n S_n^z = 1$, for the computational convenience.

Now, we deduce the effective Hamiltonian within the above restricted Hilbert space. To this end, we further take into account the effect of states consisting of three triplet dimers within the second order perturbation theory, as the number of the triplet dimers is not conserved in this system. In other words, we integrate the process into the effective Hamiltonian so that the scattering matrix elements between the two triplet states, $\langle b_{q_1, q_2} | \mathcal{H} | b_{q'_1, q'_2} \rangle$, and the diagonal elements, $\langle b_{q_1, q_2} | \mathcal{H} | b_{q_1, q_2} \rangle$, are renormalized. Then, we diagonalize numerically the effective Hamiltonian matrix and obtain the excitation spectrum and the dynamic structure factor $\mathcal{S}^{+-}(Q, \omega)$ defined by

$$\mathcal{S}^{+-}(Q, \omega) \equiv \frac{1}{2\pi} \int_{-\infty}^{\infty} dt e^{-i\omega t} \langle 0 | S_Q^- S_Q^+(t) | 0 \rangle, \quad (3.5)$$

where

$$S_Q^{\pm} = S_Q^x \pm i S_Q^y. \quad (3.6)$$

Here we note that $\mathcal{S}^{+-}(Q, \omega) = 2\mathcal{S}^{zz}(Q, \omega)$ since the system has the rotational invariance.¹⁵⁾

It is worth noticing that, in our variational calculation, the off-diagonal elements of the Hamiltonian $\langle b_{q_1, q_2} | \mathcal{H} | a_Q \rangle$'s vanish at $Q = \pi/2$ so that $|a_Q\rangle$ becomes an exact eigenstate in this case. Reminding the fact that we assume the complete singlet dimer ground state, which is true if the parameters are on the disorder line, we see that our variational calculation yields an exact solution at $Q = \pi/2$ and on the disorder line. It is also remarkable to note that eq. (3.5) suggests the spectral weights of $\mathcal{S}^{+-}(Q, \omega)$ depend on how much the state $|a_Q\rangle$ is mixed in the excited states. In fact, a contribution of the state $|a_Q\rangle$ seems to dominate $\mathcal{S}^{+-}(Q, \omega)$ as far as the ground state has the dimer order.

Next, we discuss the excitation spectra which are shown by the three dashed curves in Fig. 2 (b) and (c). These are, hereafter, denoted as $\omega_B(Q)$, $\omega_L(Q)$, and $\omega_U(Q)$ in the order of their energy, i.e., $\omega_B(Q) < \omega_L(Q) < \omega_U(Q)$. The excitation spectrum forms the continuum band in the region $\omega_L(Q) < \omega < \omega_U(Q)$, while the lowest energy state is a bound state, whose dispersion curve $\omega_B(Q)$ agrees well with the lowest energy poles of $\mathcal{S}^{zz}(Q, \omega)$ for $\delta \geq 0.2$.

It is quite reasonable that, the dispersion of all modes continuously tends to vanish with approaching the independent dimer point $\delta = 1$ and $j = 0$, where the ground state consists of the $N/2$ independent dimers. In this limit, the first and the second excited states include, respectively, one local triplet and two local triplets in the singlet dimer background. Considering these, we conclude that the continuum band consists of two local triplets: the upper and lower bounds are states where two triplets are located in the nn sites and in the distant sites, respectively. As is seen in Fig. 2 the dispersion

curve for the former coincides well with the numerical result while that of the latter does not. We feel that, in order to obtain a reasonable result for the lower bound, the restriction of our variational calculation that the triplet is on nn sites must be released. In this sense our result becomes worse when δ approaches zero.

As was mentioned above, in the limit of the MG point, ($\delta = 0, j = 1/2$), our perturbative approach fails to reproduce the continuum band obtained by the numerical diagonalization. For this case, the system possesses the full translational symmetry, giving rise to the degeneracy of the ground states. In other words, an elementary excitation in this case is not such a local triplet state but a spin-1/2 domain wall propagating on the lattice, as was shown by Shastry and Sutherland.¹²⁾ In fact, we show in Fig. 2 (d) their result for the upper and the lower bound of the continuum band with the dash-dotted curve. In this limit, we see the bound state in the vicinity of $Q = \pi/2$, which is the same as the one discussed above, although it merges into the continuum band at the wavevectors $Q = 0.36\pi$ and 0.64π .

In our variational approach, one additional bound state is observed in the energy spectrum. It lies between the lowest bound state and the lower boundary of the two triplet continuum as shown in Fig. 5. No correspondence is found in the result of the numerical diagonalization. But it has only the quite small contribution to the scattering intensity. Perhaps it is caused by the strong restriction for the Hilbert space in our variational calculation, i.e. , each pair of spins that forms the local triplet state are bound more gradually in space, not bound strongly on the nearest neighbour sites.

In conclusion, we see that our variational calculation gives us a reasonable explanation for the dispersion for the bound state as well as the continuum band obtained in the numerical calculation except for its lower boundary. Now, we turn to the wavevector dependence of their intensities on the lowest energy states. The behavior of the intensities coincides with that of the numerical result, as shown in Fig. 6, not only qualitatively but also quantitatively, although this coincidence becomes worse when the parameters tend to the MG point. Decreasing δ along the disorder line, we find the spectral weight of the lower energy mode decreases while that of the higher energy mode gets the intensity, except at $Q = \pi/2$ where only the lower energy mode has the intensity. This tendency is again consistent with the result of the numerical calculation.

§4. Conclusion

In conclusion, we have found that in the $S = 1/2$ antiferromagnetic chain with alternating nn interactions and competing nnn interactions, the dynamic correlation function shows characteristic features due to the dimer order in the ground state: (1) The ground state is the disordered state so that the static structure factor, which is obtained by an integration of $\mathcal{S}^{zz}(Q, \omega)$ with respect to ω , has a relatively high intensity even at wavevectors other than $Q = \pi$. This is marked contrast to the case in the spin-fluid state. (2) The width of $\mathcal{S}^{zz}(Q, \omega)$ at $Q = \pi/2$ becomes narrow as the disorder line is ap-

proached and eventually reaches zero at the disorder line. (3) The lowest pole for each wavevector splits off from the continuum band. We elucidated the nature of these states by the variational calculation assuming the triplet states based on the physical picture, and confirmed the facts mentioned above.

All the behavior observed in our results is consistent with the experimental observation of NIS.^{2,3)} This suggests that the parameters of CuGeO₃ are close to those on the disorder line. We believe that the reason why the NIS result shows very different characteristic behavior from what we expect for a small dimerization in the nn spin-Peierls system is a manifestation of the important role played by the rather large competing nnn interaction. We have not aimed at comparing quantitatively our theoretical result with the experimental result of CuGeO₃ in this paper, because we feel that the following issues should be considered for a quantitative comparison.

First we should throw light on the effect of the inter-chain interactions, since they are not so weak and said to be only one order of magnitude smaller than the intra-chain interactions. We believe, however, that the effect is reduced by singlet fluctuations caused by the rather large nnn interactions. Second a possibility that the dimerized lattice distortion can relax according to the spin state should be considered. If the lattice distortion follows completely the spin behavior, our Hamiltonian is inadequate in the sense that the distortion is treated as rigid. In such a case a soliton state like the one discussed for the magnetic ground states in high fields^{16,17)} may be a proper excited state. In this situation, information for the phonon is highly desired. In any case this is an interesting as well as a challenging problem for our future study. Lastly, the condition for the bound state to exist should be clarified from both experimental and theoretical sides.

At the final stage of our study, we have been notified that Yokoyama and Saiga¹⁸⁾ have studied the same problem using the same method. They claimed for CuGeO₃ rather large value of j keeping a small value of δ , which is consistent with our conclusion in the sense that, in order to see characteristic features of the spin correlation function, the system should be close to the disorder line. We hope that these calculations stimulate further experimental work of NIS to elucidate the nature of the bound state as well as the continuum band, which enable us a quantitative comparison with theoretical calculations.

Acknowledgments

The authors would like to thank Professor M. Arai and Mr. M. Fujita of KEK for valuable discussions concerning their experiment, which have encouraged them throughout this work. Thanks are also due to Professor H. J. Mikeska of Hannover University for his useful comments. Our computer programs for the numerical diagonalization of the Hamiltonian is based on the subroutine package, TITPACK Ver.2, coded by Professor H. Nishimori. The computation in this work has been done using the facilities of the Supercomputer Center, Institute for Solid State Physics, University of Tokyo.

References

- [1] For review see, J. P. Boucher and L. P. Regnault: *J. Phys. (France)* **6** (1996) 1939.
- [2] M. Arai , M. Fujita , M. Motokawa, J. Akimitsu and S. M. Bennington: *Phys. Rev. Lett.* **77** (1996) 3649.
- [3] M. Ain, J. E. Lorenzo, L. P. Regnault, G. Dhaleen, A. Revcolevschi, B. Hennion and Th. Jolicoeur : *Phys. Rev. Lett.* **78** (1997) 1560.
- [4] For review see, J. W. Bray, L. V. Interrante, I. S. Jacobs and J. C. Bonner: *Extended Linear Chain Compounds*, J. S. Miller ed. (Plenum Press, New York, 1982) Vol. 3. p.353.
- [5] A preliminary result of the present work has been reported at ICM'97, Australia.
- [6] J. Riera and A. Dobry: *Phys. Rev. B* **51** (1995) 16098.
- [7] G. Castilla , S. Chakravarty and V. J. Emery : *Phys. Rev. Lett.* **75** (1995) 1823.
- [8] R. Chitra , S. Pati , H. R. Krishnamurthy, D. Sen and S. Ramasesha : *Phys. Rev. B* **52** (1995) 6581.
- [9] S. Brehmer, H.-J. Mikeska and U. Neugebauer: *J. Phys.; Cond. Mat.* **8** (1996) 7161.
- [10] T. Tonegawa and I. Harada: *J. Phys. Soc. Jpn.* **56** (1987) 2153; T. Tonegawa, I. Harada and M. Kaburagi : *ibid.* **61** (1992) 4665.
- [11] K. Okamoto and K. Nomura : *Phys. Lett. A* **169** (1992) 433.
- [12] B. S. Shastry and B. Sutherland: *Phys. Rev. Lett.* **47** (1981) 964.
- [13] E.R. Gagliano and C. A. Balseiro : *Phys. Rev. Lett.* **59** (1987) 2999.
- [14] W. J. Caspers and W. Magnus: *Phys. Lett.* **88A** (1982) 103.
- [15] We have calculated $\frac{1}{2}\mathcal{S}^{+-}(Q, \omega)$ rather than $\mathcal{S}^{zz}(Q, \omega)$ because of the convenience. It is, however, noted that these correlation functions are the same in the present isotropic system.
- [16] I. Harada and A. Kotani: *J. Phys. Soc. Jpn.* **51** (1982) 1737.
- [17] V. Kiryukhin, B. Keimer, J. P. Hill and A. Vigliante: *Phys. Rev. Lett.* **76** (1996) 4608.
- [18] H. Yokoyama and Y. Saiga: to be published in *J. Phys. Soc. Jpn.*

Figure Captions

Fig. 1 Ground-state phase diagram in the parameter space spanned by the alternation parameter δ and the competing next nearest neighbor interaction j . The solid line shows the spin-fluid (SF) phase without a spin gap. Other region is the dimer (D) phase with the spin gap. The disorder line is denoted by the dashed line and the Majumdar-Ghosh (MG) point is indicated.

Fig. 2 Dynamic spin correlation function of the finite spin system ($N = 24$), $\mathcal{S}^{zz}(Q, \omega)$, for representative values of parameters, δ and j . In (a) the dash-dotted curves show the rigorous upper and lower boundaries of the triplet band, while in (b), (c) the approximate dispersion curves of the traveling triplet dimer in the singlet-dimer background are represented by the dashed curves. (See text.) In (d), the dash-dotted curves show the two-particle scattering continuum of the $S = 1/2$ domain walls¹²⁾

Fig. 3 Intensity ratio of the lowest energy poles, $\mathcal{S}^{zz}(Q, \omega_B)/\mathcal{S}^{zz}(\pi, \omega_B)$, for $j = 0.3$ and representative values of δ as a function of the wavevector Q .

Fig. 4 Two types of triplet states adopted to construct the trial wave functions. In each state, the two arrows form the triplet state with $S_n^z + S_{n+1}^z = 1$ while the solid rectangle denotes the triplet pair with $S_n^z + S_{n+1}^z = 0$. The solid ellipse shows the singlet pair which is the same as in the ground state.

Fig. 5 Triplet excitation spectra for $j = 0.3$ and $\delta = 0.4$. The solid lines represent the result obtained by the variational calculation while the open diamonds denote the result obtained by the numerical diagonalization for the finite system ($N = 24$). The shaded area denotes the continuum band obtained by the variational calculation.

Fig. 6 Wavevector dependence of the spectral weight on the lowest excited mode $\omega_B(Q)$. The numerical results of the finite chain ($N = 24$) for $j = 0.1$ and $\delta = 0.8$, $j = 0.3$ and $\delta = 0.4$, and $j = 0.4$ and $\delta = 0.2$ are depicted with the circles, the diamonds, and the triangles, respectively. The broken lines are to guide the reader's eye. The solid lines denote the variational results.

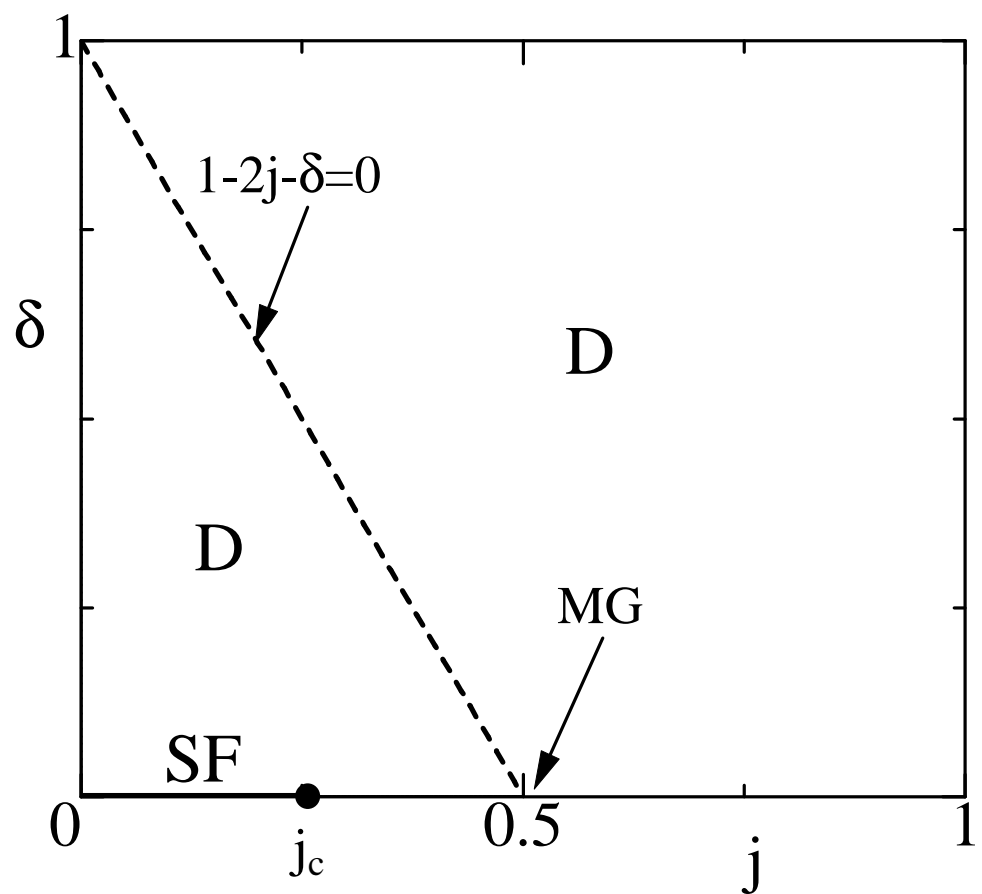


Fig. 1

Mori, Harada, Tonegawa

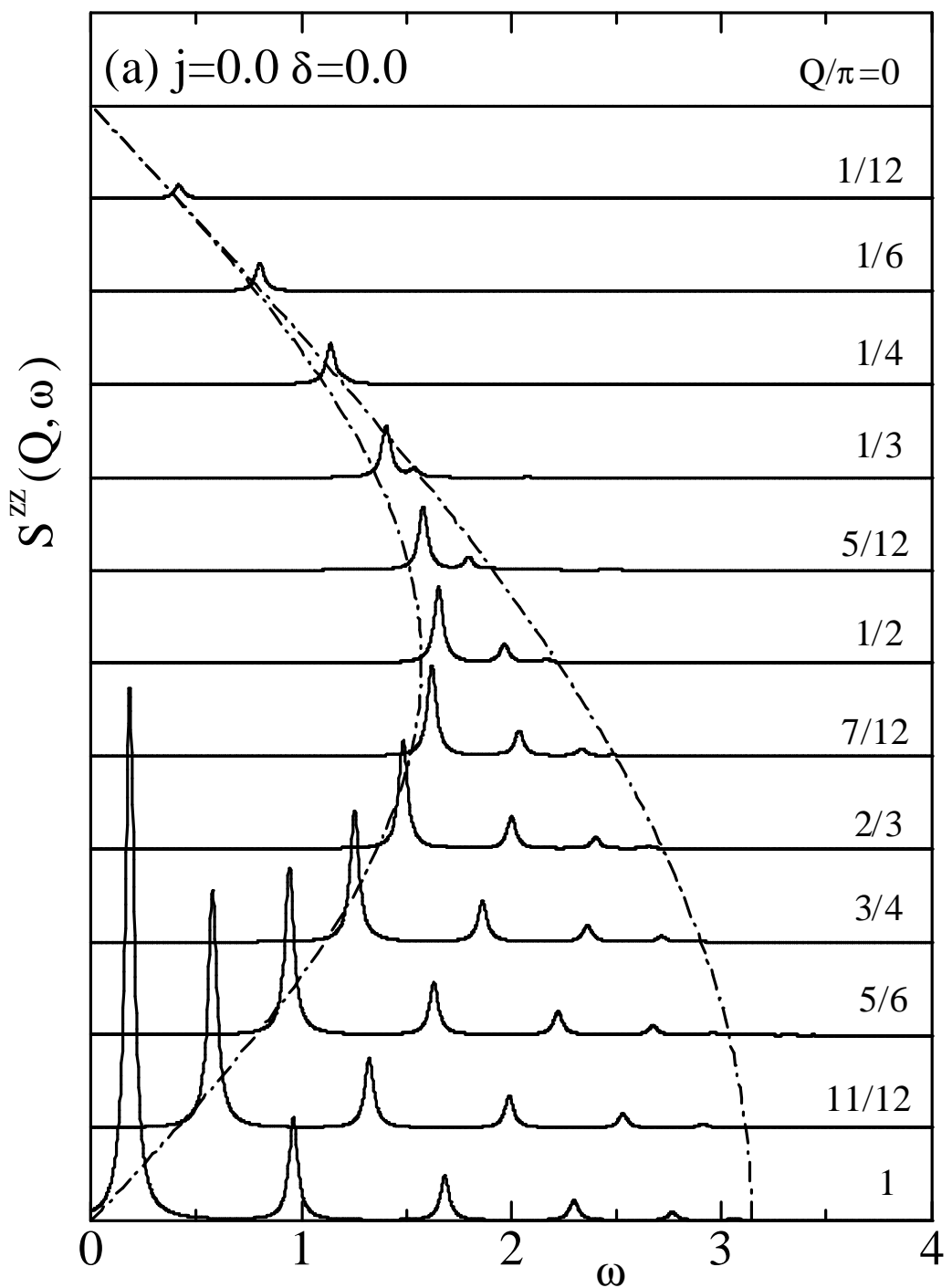


Fig.2 (a)

Mori, Harada, & Tonegawa

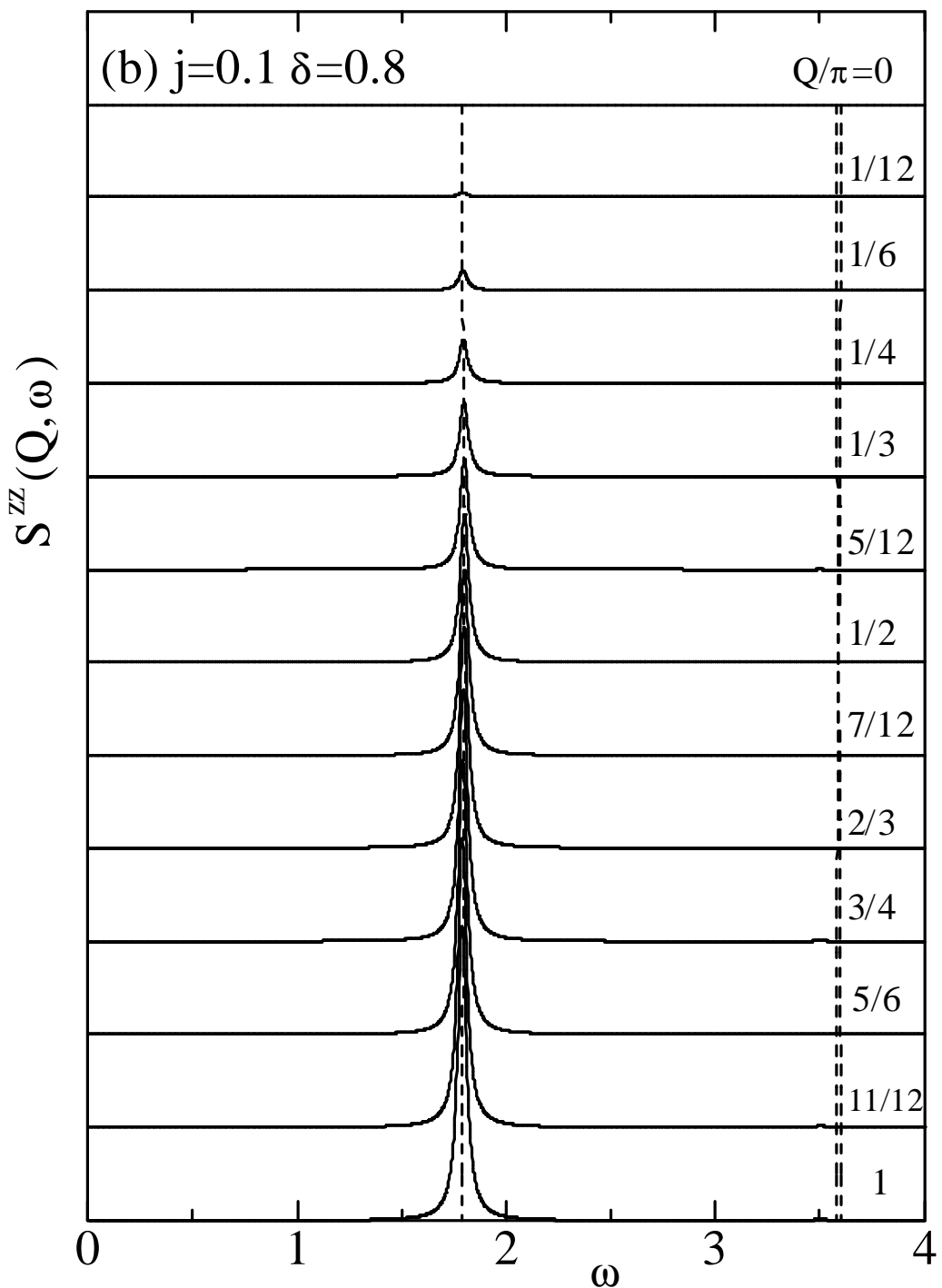


Fig.2 (b)

Mori, Harada, & Tonegawa

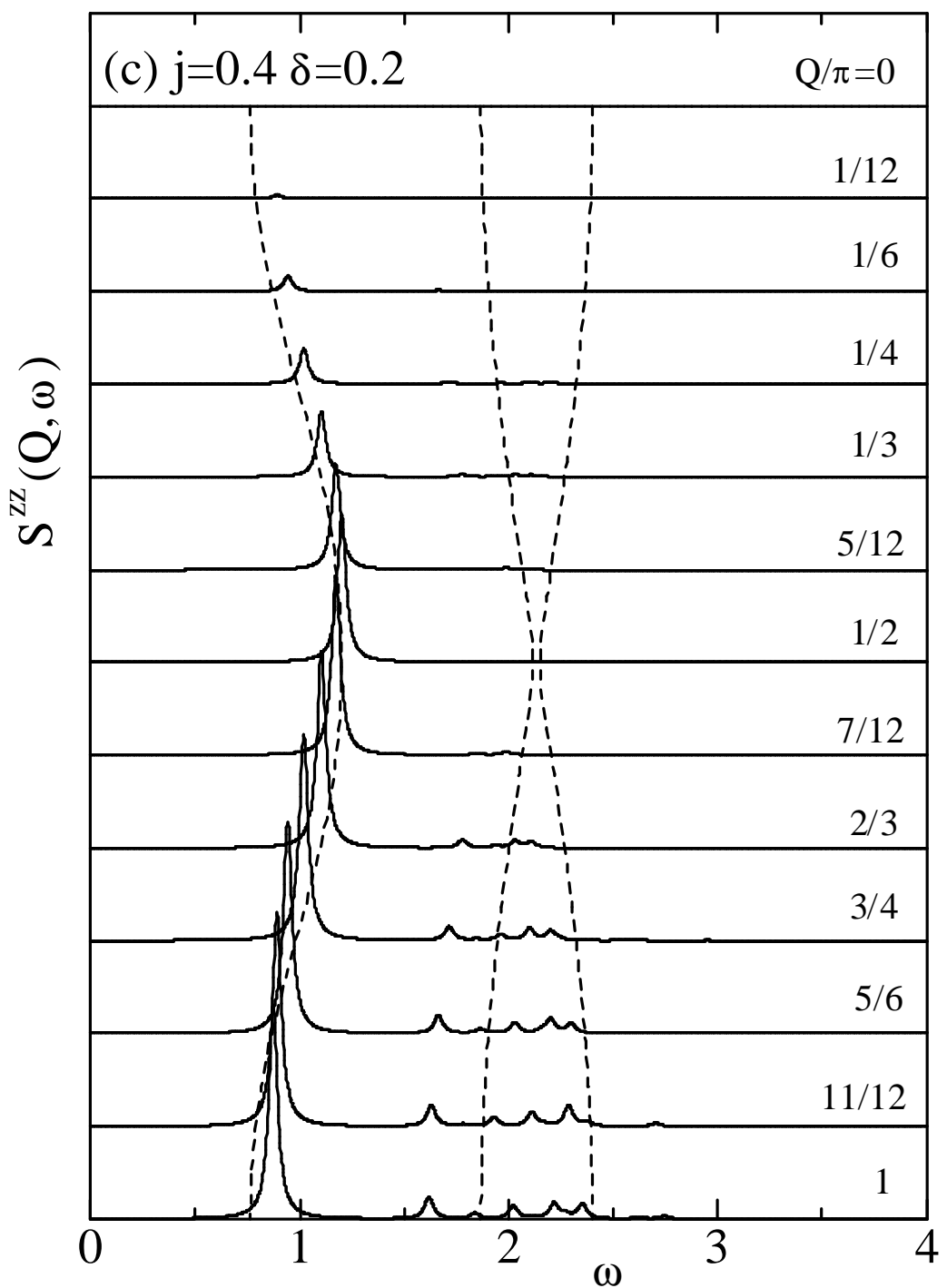


Fig.2 (c)

Mori, Harada, & Tonegawa

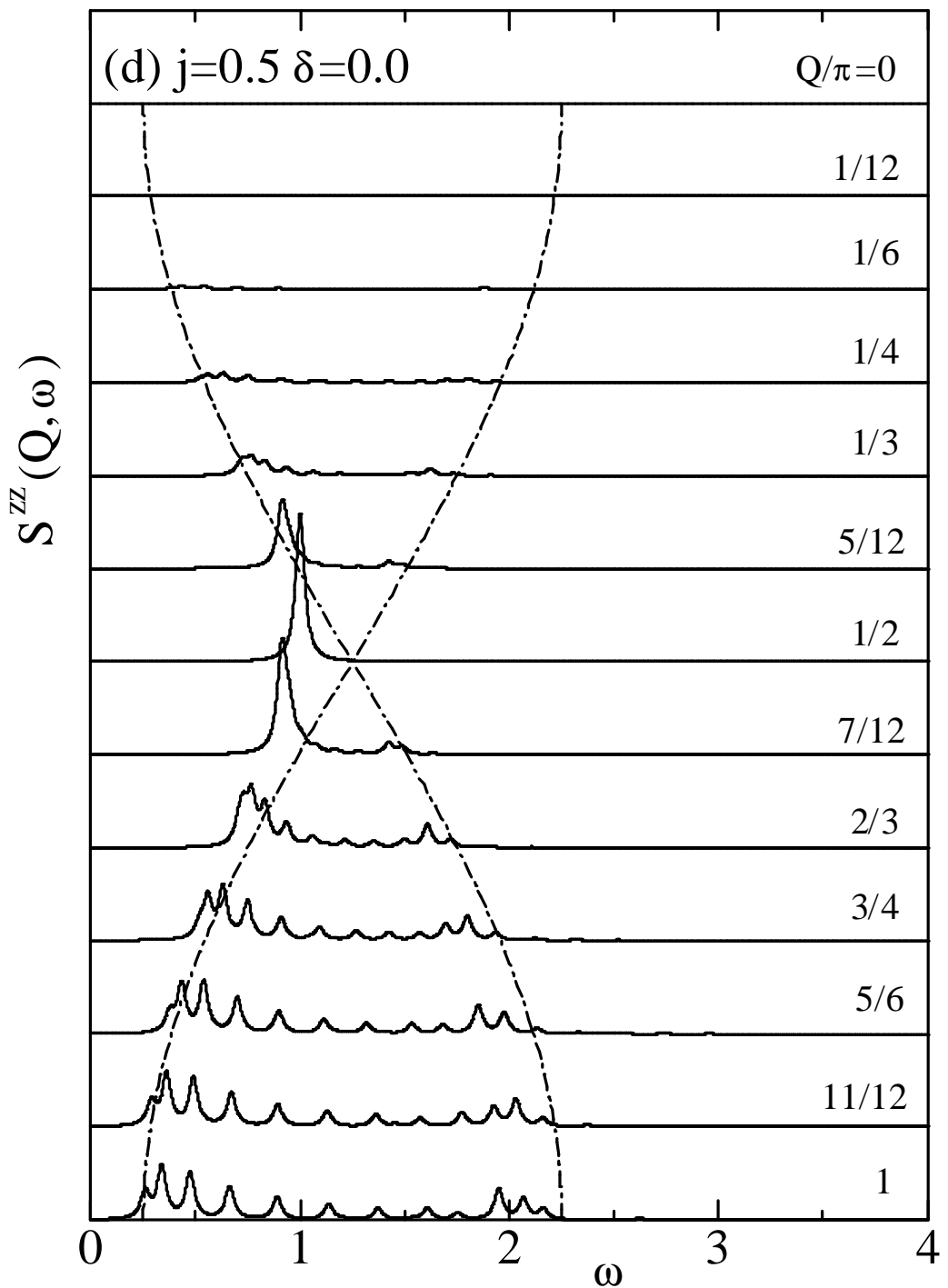


Fig. 2(d)

Mori, Harada, & Tonegawa

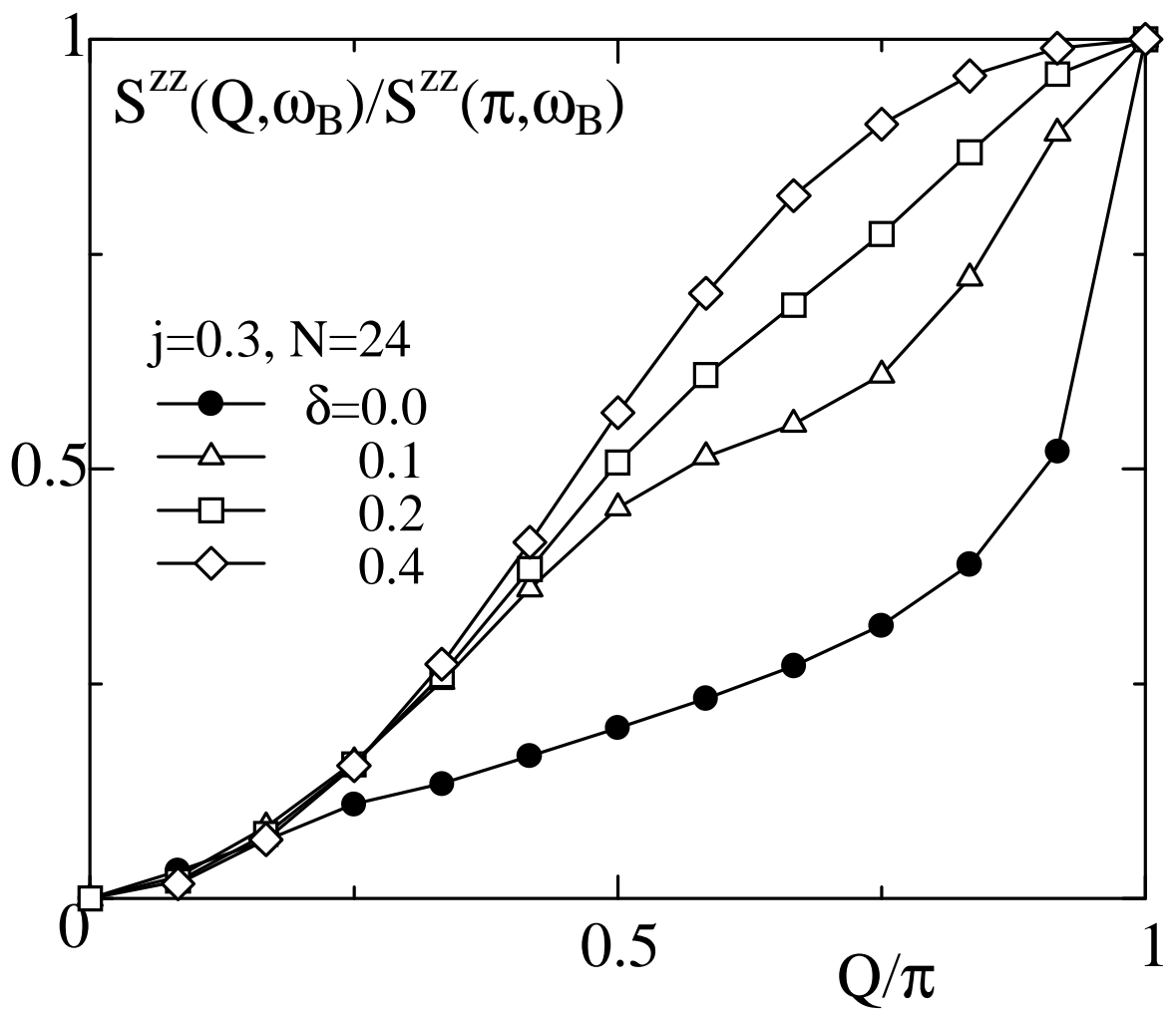


Fig. 3

Mori, Harada, Tonegawa

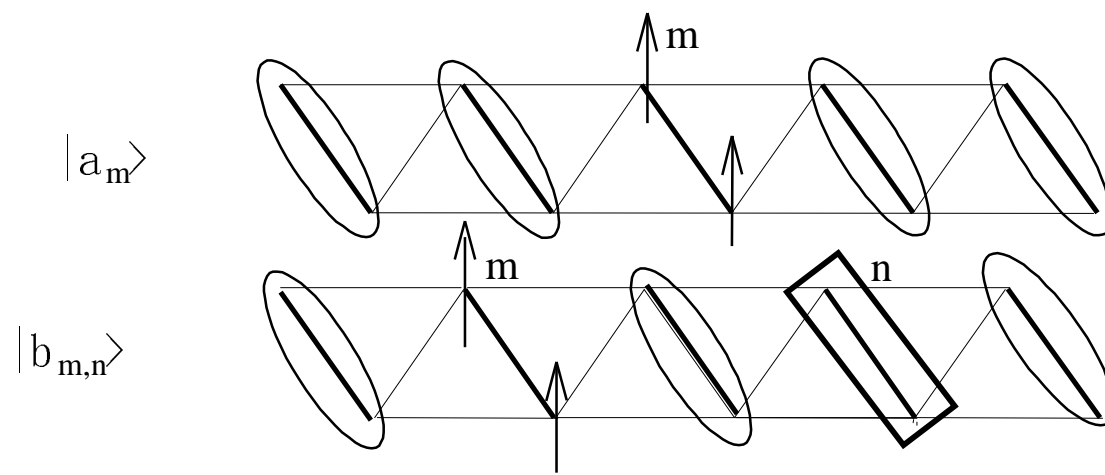


Fig.4

Mori, Harada, & Tonegawa

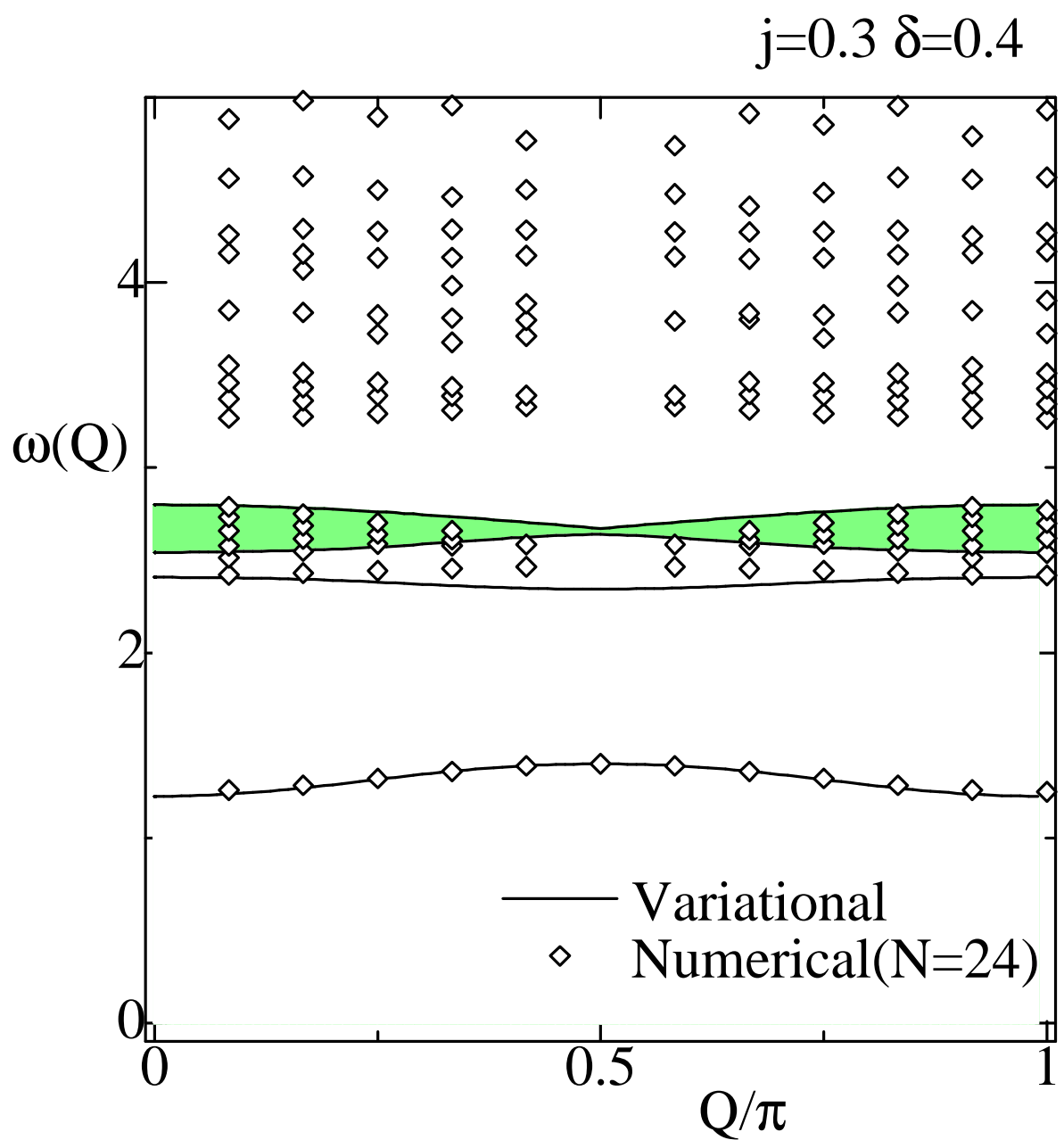


Fig. 5

Mori, Harada, & Tonegawa

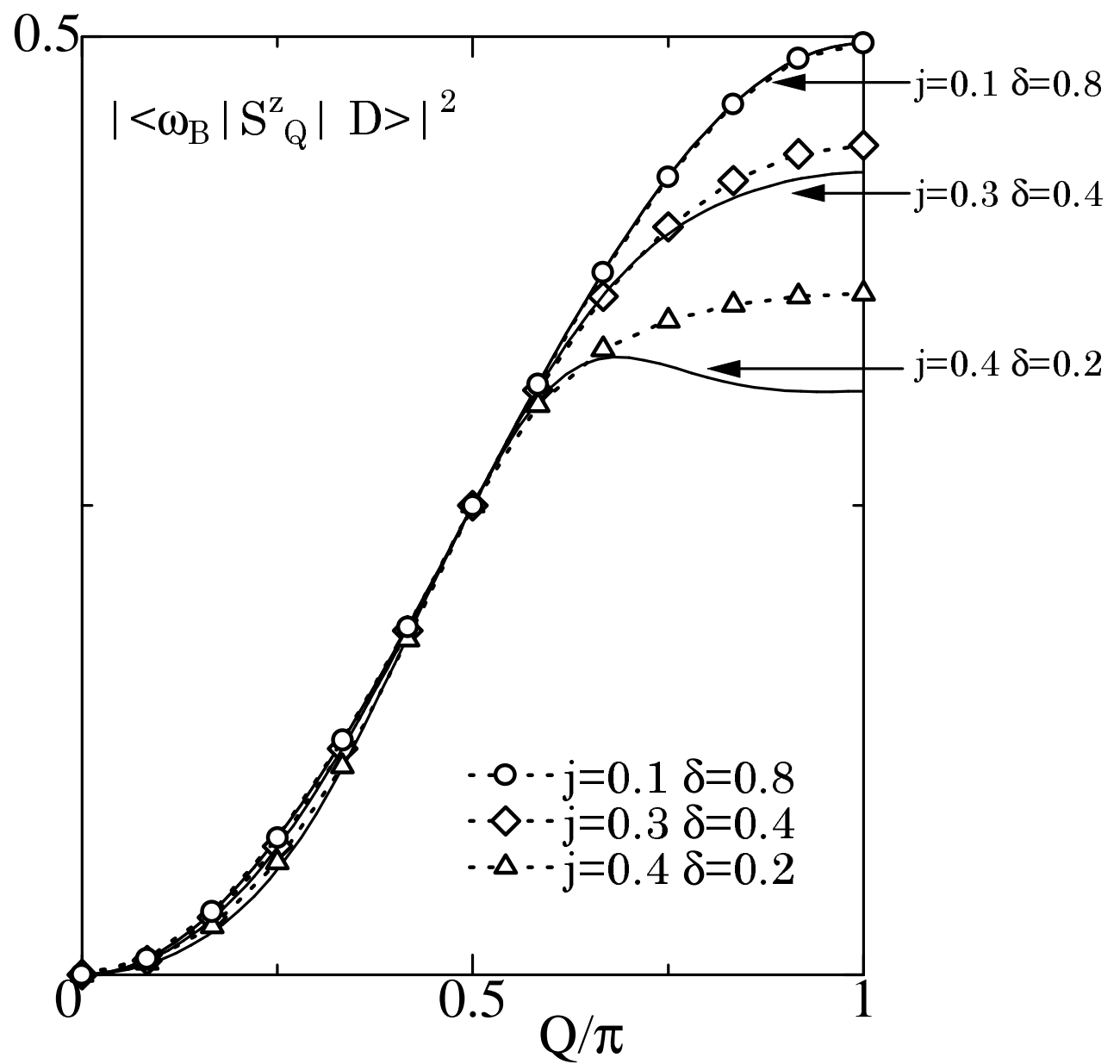


Fig. 6

Mori, Harada, & Tonegawa